

## INTERPLANETARY SCINTILLATIONS. II. OBSERVATIONS

M. H. COHEN,\* E. J. GUNDERMANN, H. E. HARDEBECK,† AND L. E. SHARP  
Center for Radiophysics and Space Research, Cornell University, Ithaca, New York

Received July 5, 1966

### ABSTRACT

Observations of interplanetary scintillations have yielded the statistical quantities needed to fix the scattering regime. The observations fit the theory rather well and show that the fluctuations in electron density have a correlation length of 110 km. The rms density variation is given approximately by  $\Delta n = 0.14r^{-2} \text{ cm}^{-3}$  ( $r$  = radial distance from the Sun in astronomical units) for  $0.2 < r < 0.9$ , in the equatorial region of the corona, during September–November, 1965. The effect of angular extension of the source on the fluctuation spectrum of scintillations is discussed, and it is shown that the sources 3C 138 and 3C 273 have components with angular size  $\sim 0''.1$  and  $\lesssim 0''.02$ , respectively.

### I. INTRODUCTION

Radio scintillations due to irregularities in the solar wind were first observed systematically by Hewish, Scott, and Wills (1964), although they had earlier been invoked by Douglas and Smith (Douglas 1964) as a possible explanation for some of the features of Jovian bursts. Hewish *et al.* (1964) observed several dozen sources at 178 MHz, and made estimates of scale and velocity of the irregularities, as well as of limits to the diameter of the sources. The work has since been extended to lower frequencies and to simultaneous observations over an extended base line (Hewish and Okoye 1965; Hewish, Dennison, and Pilkington 1966), and also to higher frequencies and observations over a wider range of solar elongation (Cohen 1965).

The observations reported in the present paper were recorded digitally, and various statistical quantities, such as the power spectrum, were computed. These allow a quantitative approach to the interpretation of the observations. For example, we do not have to appeal to the ill-defined concept of "fully developed fluctuations" to demonstrate that we are in the "far field." More importantly, however, we can be more precise about the limits to angular diameter and can even give specific dimensions in some cases.

Interpretation of the observations requires a knowledge of the scattering regime, since the phenomenon looks very different in different limiting cases. In a companion paper (Salpeter 1966; hereinafter referred to as "[I]") the theory of scattering by a random phase-changing screen is reviewed and extended. In the next section of this paper we give a brief summary of those theoretical results we need for comparison with our observations. In §§ III and IV the observational data are summarized and compared with the theory. The observations fit the theory reasonably well, and we are able to fix the scattering regime. We are then in a position to discuss the parameters of the screen: distance, scale, and electron density. We find that the scale is 110 km, and that the rms fluctuation in electron density is about 0.02 of the ambient density.

In § VI we give a brief discussion of the effect of a finite source diameter and apply the analysis to observations of the sources 3C 138 and 3C 273. This interpretation gives dimensions for 3C 138 and 3C 273 of  $\sim 0''.1$  and  $\lesssim 0''.02$ , respectively. Some effects of finite screen thickness are considered in § VII. The rapid reduction in index when a source comes very close to the Sun is most likely an effect of the finite screen thickness.

### II. SUMMARY OF THE RELEVANT THEORY

A wave passing through a thin, one-dimensional, random, phase-changing screen has phase deviations  $\phi(x)$ . The mean square phase deviation is  $\phi_0^2$ , and  $\phi(x)$  has an auto-

\* Present address: University of California at San Diego, La Jolla, California.

† Present address: University of Pennsylvania, Philadelphia, Pennsylvania.

correlation function  $\phi_0^2 \rho(r)$  and (power) spectrum  $\phi^2(q)$  [I, eqs. (1)–(3)]. The correlation length, or scale,  $a$ , is defined as the reciprocal (square root) second moment of  $\phi^2(q)$ . For example, a Gaussian screen would have

$$\rho(r) = e^{-(r/a)^2/2},$$

$$\phi^2(q) = (2\pi)^{-1/2} a \phi_0^2 e^{-(qa)^2/2},$$

and  $a^2 = q_0^{-2} = \sqrt{\frac{3}{2}} Q_0^{-2}$ , where  $q_0^2$  and  $Q_0^4$  are the second and fourth moments of  $\phi^2(q)$ . The scale is given by the  $-2.17$ -db point on either  $\rho(r)$  or  $\phi^2(q)$ .

The observer measures the intensity  $I(x)$  (with mean value  $I_0$ ) on a plane parallel to the screen, at distance  $z$ . The observed intensity fluctuation,  $\Delta I(x) = I(x) - I_0$ , has the (power) spectrum  $M(q)$ . In practice, the observer may not measure  $I(x)$ , but rather  $I(t)$ , the intensity at one place as a function of time. If all scales move with the same velocity, then the frequency spectrum measured at one place is simply related to the spatial spectrum:  $M(f) = M(qu/2\pi)$ , where  $u$  is the velocity of the screen.

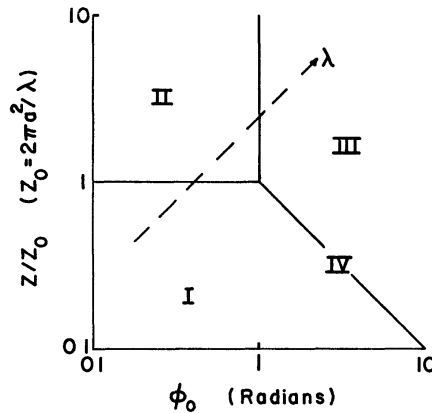


FIG 1.—Scattering regimes;  $\phi_0$  = rms phase deviation,  $a$  = scale of phase fluctuations. Observations made at different wavelengths fall along the dashed line, which is a line of constant  $\eta < 1$  [I, eq. (35)].

The character of the scintillations of a point source is controlled by two parameters,  $\phi_0$  and  $z/z_0$ , where  $z_0 = 2\pi/\lambda Q_0^2 \approx ka^2$  is the “Fresnel distance” of a “blob” ( $k = 2\pi/\lambda$ ;  $\lambda = rf$  wavelength). Figure 1 shows the four major regimes. The scintillations behave differently in the various regions, and the region must be known before any observations can be interpreted. The major results are as follows.

a) *Region I*

$$z \ll z_0 \quad \text{when} \quad \phi_0 < 1; \quad z \ll l_0 \equiv z_0/\phi_0 \quad \text{when} \quad \phi_0 > 1.$$

$$\text{Spectrum: } M(q) \approx I_0^2 (z/z_0)^2 (qa)^4 \phi^2(q);$$

$$\text{Index: } m \approx \phi_0 z/z_0.$$

The spectrum is peaked around  $q = a^{-1}$  and the index  $m$  is proportional to  $\lambda^2$ . (The index is defined as the relative rms intensity fluctuation.) There is a Gaussian distribution of intensities, and a high cross-correlation between scintillations observed at different frequencies [I, § III and X].

b) *Boundary between Regions I and II*

As the boundary  $z \sim z_0$  is approached, the position of the peak of the spectrum moves toward smaller  $q$ , and approaches the (reciprocal) Fresnel zone dimension  $\sqrt{(2\pi^2/\lambda z)}$ .

The system acts as a filter and selects wave-numbers corresponding to the Fresnel zone on the screen. As  $z$  gets bigger than  $z_0$  the  $\sin^2$  function in equation (15) of [I] becomes oscillatory inside the phase spectrum  $\phi^2(q)$  and an oscillatory  $M(q)$  is produced.

*c) Region II*

$$z \gg z_0, \quad \phi_0^2 \ll 1, \quad M(q) \approx 2I_0^2 \phi^2(q), \quad m \approx \sqrt{(2)\phi_0}.$$

The (smoothed) spectrum on the ground is the same as the spectrum of phase fluctuations in the screen, and the index is proportional to  $\lambda$ . There is a Gaussian distribution of intensities, and the cross-correlation is high provided  $\Delta f/f \equiv \frac{1}{2}(f_2 - f_1)/(f_2 + f_1) < z_0/z$  [I, §§ III and X].

*d) Region III*

$$z \gg l_0, \quad \phi_0^2 \gg 1, \quad M(q) \approx \exp\left[-\left(\frac{qa}{2\phi_0}\right)^2\right], \quad m \approx 1.$$

The spectrum has a Gaussian shape, and its width  $\sqrt{(2)\phi_0}/a$  is proportional to  $\lambda$ . The index is on the order of unity. There is a "Rice" distribution of amplitudes (exponential distribution of intensities when  $z \gg z_0$ ) and the cross-correlation is low unless  $\Delta f/f < (z_0/z)\phi_0^{-2}$  [I, §§ III, IV, and X].

*e) Region IV. Boundary between Regions I and III*

$$z \sim l_0 \ll z_0.$$

The scintillations are dominated by sharp spikes which are the focal spots. The distribution function is highly skewed, and there is a low correlation between scintillations at different frequencies unless  $\Delta f/f < \phi_0^{-1/3}$ . The spectrum width is a rapid function of  $\lambda$ , increasing from approximately  $a^{-1}$  in Region I to  $\sqrt{(2)\phi_0} a^{-1}$  in Region III (cf. Fig. 3 of [I]). The index is bigger than unity [I, §§ IV and X].

### III. OBSERVATIONS, DATA ANALYSIS, AND SOME SAMPLE RESULTS

Observations of interplanetary scintillations are being made with the 1000-foot telescope at the Arecibo Ionospheric Observatory. Many sources have been observed, but we shall use only results from 3C 138, 273, 287, 286, and 298. The general results will be given in another paper.

A typical observation consisted of 5 min of looking on the source and then 5 min looking at a nearby control region. Three frequencies were generally used: 195, 430, and 611 MHz, with band widths of 1, 3, and 9 MHz, respectively. At the beginning of this series of observations the data were recorded digitally at 10 samples per second (s/s), but when higher-frequency components in the fluctuation spectrum were discovered the sampling rate was increased to 25 s/s, and occasional records were taken at 100 s/s. Figure 2 shows some sample observations.

In every case the analogue records were inspected, and a preliminary value for scintillation index was computed by estimating  $\sigma$ , the rms fluctuation level, on and off the source. The index  $m$  is found from

$$m^2 = \frac{\sigma_{\text{ON}}^2 - \sigma_{\text{OFF}}^2}{T_A^2}, \quad (1)$$

where  $T_A$  is the antenna temperature of the source.

The digital records are used to compute the statistical quantities for the cases of interest. In the most general case the data processing contains the following elements: (1) lightning elimination; (2) low-pass filter; (3) high-pass filter; (4) autocorrelation function; (5) power spectrum; (6) cross-correlation function; (7) distribution function. These

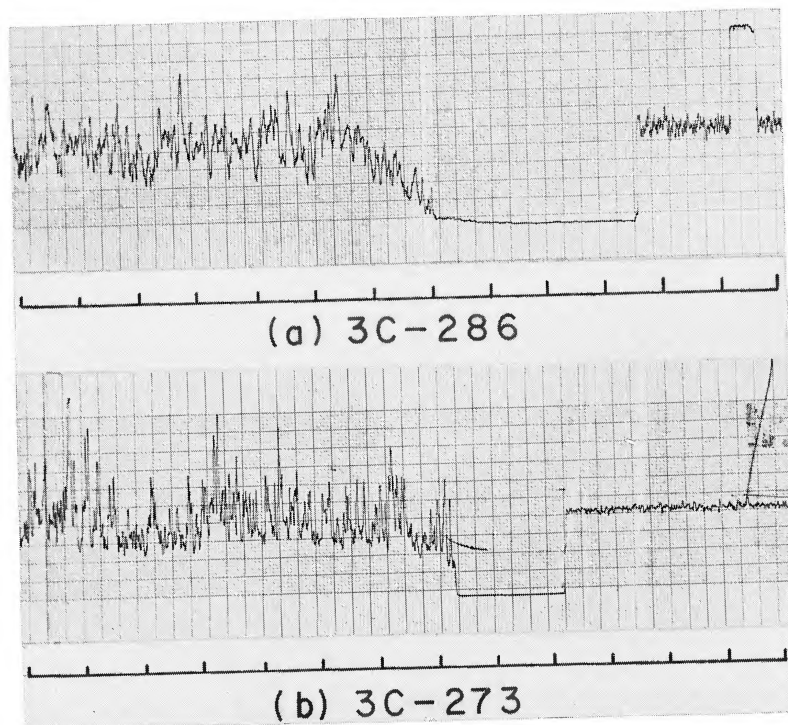


FIG. 2.—Scintillation records, on and then off the source. The zero has been reset in both cases, to bring the “off” record to midscale. One minute marks are shown. (a) 3C 286, Oct. 3, 1965, 430 MHz,  $\tau \approx 0.1$ ,  $\epsilon \approx 30^\circ$ ; (b) 3C 273, Sept. 26, 1965, 430 MHz,  $\tau \approx 0.1$ ,  $\epsilon \approx 5^\circ$ .

seven elements are discussed very briefly, and then some examples and discussion are given.

1. The lightning-elimination program tests for the slope between adjacent points and rejects a short section of data when the slope is excessive. The missing data are replaced by a linear interpolation between the surviving sections.

2. The low-pass filter consists of smoothing and decimation, as discussed by Blackman and Tukey (1958). Even when it is known a priori that the fluctuation spectrum is narrow, say all within 2 c/s, experience has shown that it is desirable to take data at 25 s/s or faster. A short RC time constant may then be used, and lightning (and some interference) can be eliminated with negligible loss of data. The lightning-free data can then be filtered to give a total spectrum of 5 c/s or less, as desired. Undesirable aliases can also be eliminated more easily if digital filtering is used in addition to the normal RC filter.

3. The high-pass filter consists of subtracting a running mean from the data. The end sections of the averaging block are weighted less than the middle to reduce side lobes. A cutoff frequency on the order of 0.1 c/s is generally used, to eliminate ionospheric effects.

4, 5. The autocorrelation function and power spectrum are computed according to procedures given by Blackman and Tukey (1958). The correlation function is computed to a maximum lag  $\tau_m$ , which determines the spectral resolution. The computed spectrum is an estimate of the aliased true spectrum convolved with the spectral window function. The Hanning function is generally used.

6. The cross-correlation function between records at different observing frequencies is computed. The cross-power spectrum may also be computed.

7. The distribution function of the intensity fluctuations is computed. Moments of the distribution, through fourth order, are tabulated.

#### a) Spectrum

In practice the power spectrum is normally computed for both the "on" and "off" records of a source. The spectrum of the scintillations is then found by subtracting the "off" from the "on" spectrum, and correcting for the filter. In principle the "off" spectrum should first be corrected to allow for the increase in thermal fluctuations due to the source temperature's being added to the receiver noise. It has been found, however, that the correction is usually small and insignificant. It has not been applied to the data used in this paper.

Figure 3 shows some scintillation spectra for very narrow sources for the weak scattering case, with elongation  $\epsilon \geq 20^\circ$ . The point at zero frequency has been omitted since the filtering removes the d.c. component. In all cases the low-pass cutoff is at or below the first point and the ripples due to filtering are insignificant. It is thought that there are negligible ionospheric fluctuations in our data. The cutoff in most cases (although not for Figure 3, *a*, *b*, and *d*) is 0.1 c/s, and ionospheric effects typically have periods greater than 10 sec. In some cases control sources (narrow enough to show ionospheric scintillations but too wide for interplanetary scintillations) were observed at nearby times, and no unexpected ionospheric effects were observed. The vertical arrows on the abscissae of Figure 3 show the frequency at which the thermal noise is comparable with the scintillations. Eighty per cent confidence intervals are shown; these are applicable only to the left of the arrow.

The spectra are often fairly close to Gaussian, as shown in Figure 3. The (square root) second moment  $f_2$  is generally close to 0.6 c/s. For 3C 287 and 3C 286 it varied from 0.4 to 0.8 c/s. The spectrum has never been observed to have a deep depression at low frequencies.

Figure 4 shows the scintillation spectrum for a strong scattering case, with  $\epsilon = 7^\circ$ . The low-frequency peak on the 195 MHz spectrum is probably not real, since there was a comparable peak on both "on" and "off" records. It may be due to a receiver instabil-

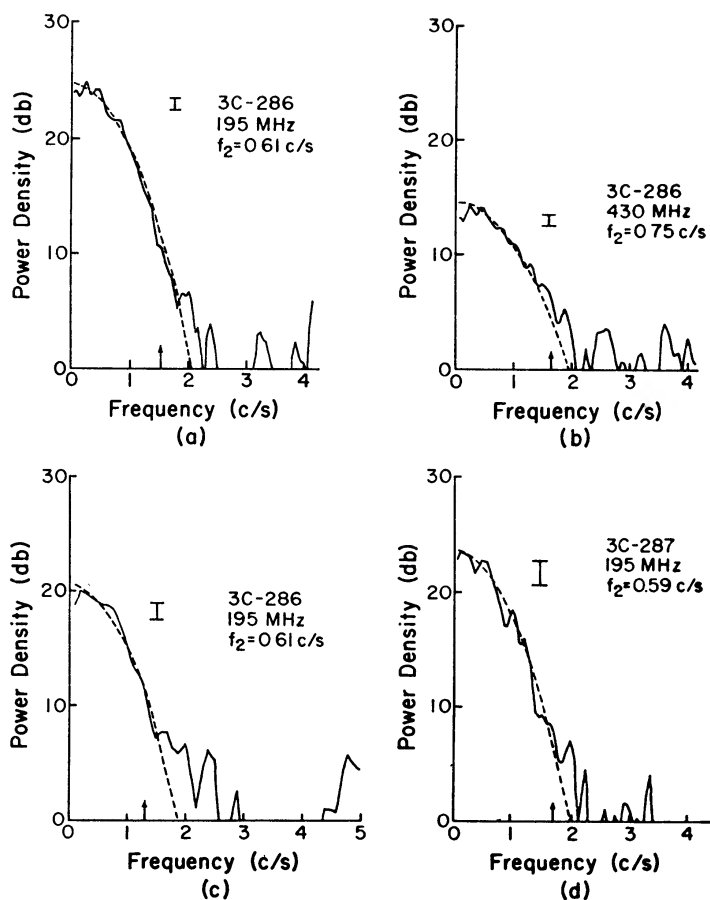


FIG. 3.—Scintillation spectra: (a) 3C 286, Oct. 3, 1965, 195 MHz, resolution 0.1 c/s 20 min observation at 25 s/s (samples per second) decimated to 8.33 s/s; (b) 3C 286, Oct. 3, 1965, 430 MHz, resolution 0.1 c/s, 20 min observation at 25 s/s decimated to 8.33 s/s; (c) 3C 286, Oct. 23, 1965, 195 MHz, resolution 0.2 c/s, 6 min observation at 100 s/s decimated to 10 s/s; (d) 3C 287 Oct 3, 1965, 195 MHz, resolution 0.1 c/s, 5 min observation at 25 s/s decimated to 8.33 s/s. The dashed curves are Gaussians with second moment  $f_2^2$  equal to the observed second moment.

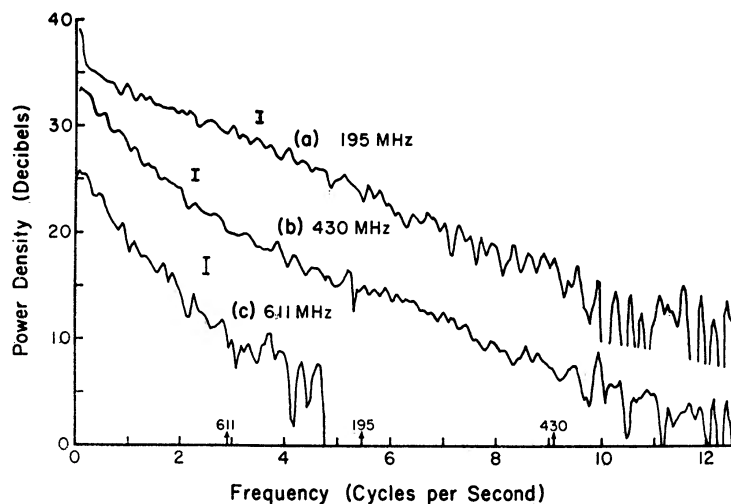


FIG. 4.—Scintillation spectrum 3C 273, Oct. 3, 1965: (a) 195 MHz, resolution 0.1 c/s, 20 min observation at 25 s/s; (b) 430 MHz, resolution 0.1 c/s, 20 min observation at 25 s/s; (c) 611 MHz, resolution 0.1 c/s, 10 min observation at 25 s/s.

ity. The spectrum falls much more slowly than a Gaussian, and can be exponential or even slower. The second moment  $f_2$  is nearly proportional to  $\lambda$ , as shown by the 3C 273 points in Figure 11 (see below).

Some autocorrelation functions and spectra have also been published for nighttime interplanetary scintillations (Cohen 1965).

### b) Scintillation Index

The scintillation index (averaged over 5 min) is a somewhat erratic quantity. It can change a factor of 2 in one day, although it hardly ever changes more than 20 per cent in 2 hours. Figure 5 shows the index, as a function of  $p = \sin \epsilon$ , for 3C 273. The variation of index with  $\lambda$  is also somewhat erratic but generally varies as  $\lambda$  to a power between 1.0 and 1.5.

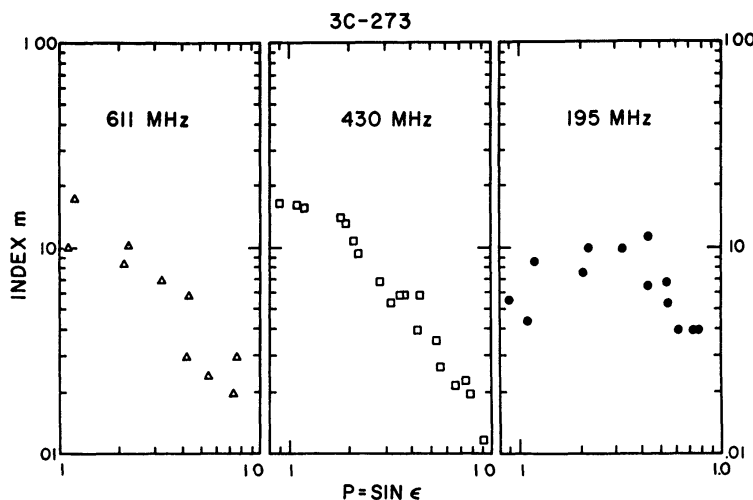


FIG. 5.—Scintillation index, 3C 273, September–November, 1965

### c) Cross-Correlation and Distribution Functions

The cross-correlation coefficient is defined as follows:

$$\Gamma_{12}(\tau) = \frac{\langle \Delta I_1(t) \Delta I_2(t + \tau) \rangle}{m_1 m_2 T_{A1} T_{A2}}$$

with  $mT_A$  given in equation (1); and 1 and 2 refer to the two frequencies being cross-correlated. This normalization attempts to correct for the thermal fluctuations, which of course are uncorrelated at the two frequencies.

Some high cross-correlation functions are shown in Figure 6, *a*, *b*, and *c*. Values (at zero lag) approaching unity have been found between 611 and 430 MHz, but the maximum observed between 430 and 195 MHz is about 0.75.

The probability distributions of the intensity fluctuations are shown in Figure 6, *d* and *e*. The normalized Gaussian distribution is shown superposed; it is seen that there is a very good fit.

When the cross-correlation is very high, as in Figure 6, *a*–*c*, the cross-power spectrum is the same (within experimental error) as the individual power spectra. This is shown in Figure 6, *f*. Computation of the power spectrum from the cross-correlation function between two close frequencies (or two polarizations, or any diversity scheme giving inde-

pendent thermal fluctuations) may in some cases yield a signal-to-noise ratio significantly higher than that obtained from one frequency alone.

A low cross-correlation function is shown in Figure 7, *a*. The function typically appears to have a bulge 1 or 2 sec wide, but no significant peaks away from zero have been found. The probability distributions of the intensity fluctuations are shown in Figure 7, *b-d*. The smooth curve superposed is the normalized Rice-squared distribution having the same second and third moments as the experimental distribution. (The skewness parameter  $\xi_3$  is listed in each case.) The experimental distribution is more peaked than the Rice-squared distribution, and the fit is not as good as the fit to the Gaussian distribution in Figure 6. (The Rice-squared distribution is discussed in the Appendix.)

The cross-correlation is independent of polarization. The feeds were usually linearly polarized, with 195 and 611 MHz perpendicular to 430 MHz.

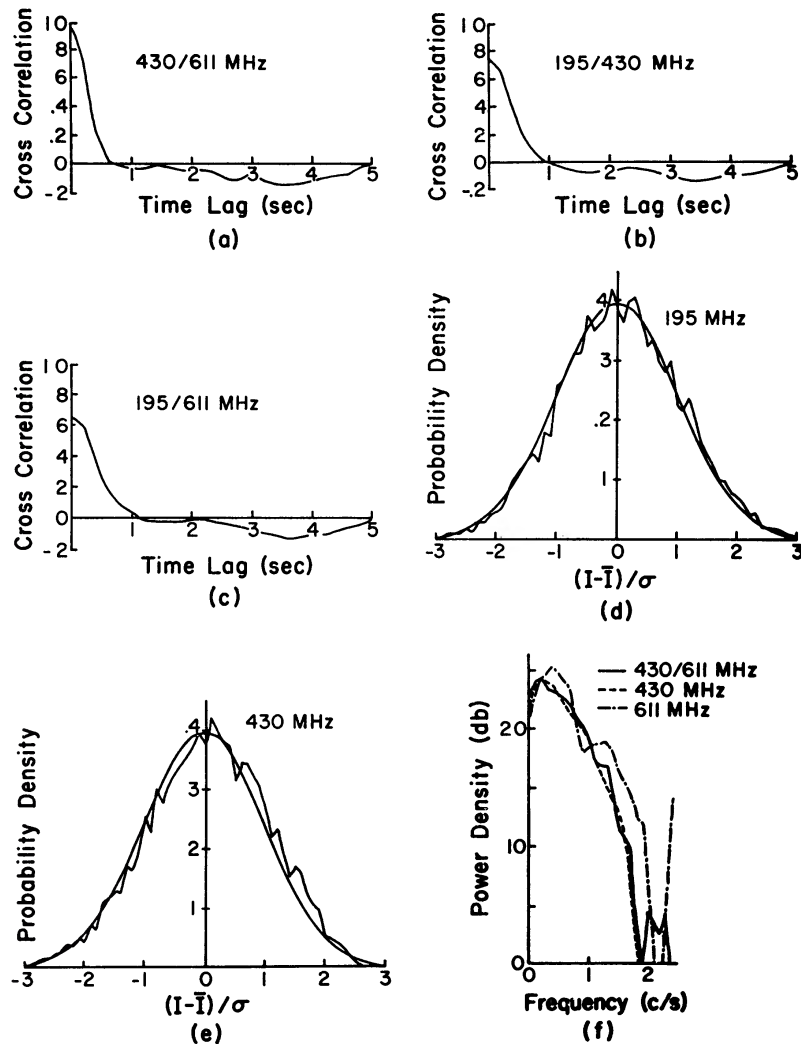


FIG 6—Weak scattering, 3C 298, Oct. 17, 1965,  $\epsilon = 20^\circ$ . Cross-correlation function (a) between 430 and 611 MHz, (b) between 195 and 430 MHz, and (c) between 195 and 611 MHz. (d) and (e) Experimental and theoretical intensity probability density functions for 195 MHz and for 430 MHz. (f) Cross-correlation spectrum between 430 and 611 MHz. Individual spectra for 430 MHz and 611 MHz are shown in broken lines.

## IV. COMPARISON OF THEORY AND OBSERVATIONS

The scintillation observations divide into two major groups, those made under weak scattering conditions ( $\epsilon > 20^\circ$ ) and those made under strong scattering conditions ( $\epsilon < 10^\circ$ ).

a)  $\epsilon > 20^\circ$

The sources 3C 287 and 286 are both known to be very narrow, with size about  $0''.1$  by  $< 0''.1$  (Adgie, Gent, Slee, Frost, Palmer, and Rowson 1965). Their scintillations have the following characteristics.

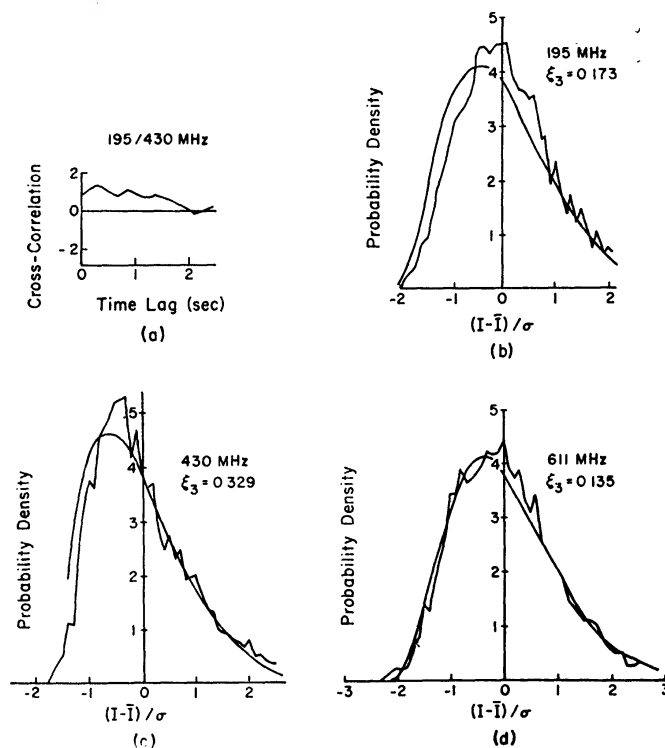


FIG. 7.—Strong scattering, 3C 273, Oct. 3, 1965,  $\epsilon = 7^\circ$ . (a) Cross-correlation function between 195 and 430 MHz. (b), (c), and (d) Experimental and theoretical intensity probability density functions for 195, 430, and 611 MHz.  $\xi_3$  is the skewness parameter.

1. The spectrum is confined to  $f \lesssim 2$  c/s. It is often close to Gaussian, with second moment  $f_2$  around 0.6 c/s. The spectrum is independent of wavelength and is essentially the same for all very narrow sources. Examples are given in Figure 3.

2. The variation of index with  $\lambda$  is somewhat erratic, but generally varies as  $\lambda$  to a power between 1.0 and 1.5.

3. The cross-correlation between scintillation fluctuations at different frequencies is high. Typical cross-correlation functions are shown in Figure 6. (3C 298 is used in Fig. 6, but any source extension should not affect the cross-correlation, provided the structure is independent of  $\lambda$ .)

4. The distribution of fluctuation intensities is closely Gaussian. Examples are shown in Figure 6.

The scattering is clearly not in Region III or IV of Figure 1. The high cross-correlation and the Gaussian distribution allow either Region I or II. The spectrum typically has at most only a minor depression near zero, which suggests that we are rather far into Region II. The index, however, does not show a clear  $\lambda^1$  dependence, but typically shows some-

thing in between  $\lambda^1$  and  $\lambda^2$ . The observations are thus not completely consistent, but the best interpretation in terms of the thin-screen theory is that we are in Region II but close to the boundary with Region I.

b)  $\epsilon < 10^\circ$

We do not have data for any source which is known a priori to be very narrow. The source 3C 273B, however, although multiple, is known to have components of size  $\leq 0.1$  (Adgie *et al.* 1965). We give its characteristics here, and discuss later the assumption that it behaves as a point source.

1. Examples of spectra are shown in Figure 4. The spectrum is roughly exponential, or flatter, with slope decreasing with  $\lambda$ . Figure 11 (see below) shows that  $f_2$  is roughly proportional to  $\lambda$ .

2. The index, for three frequencies, is shown as a function of  $p = \sin \epsilon$ , in Figure 5. The index for 3C 273B may be taken as on the order of unity (for  $\epsilon \sim 10^\circ$ ) because the observations are contaminated by the broad source 3C 273A, which has not been corrected for. (The receiver non-linearity, which is noticeable for this strong source, also reduces observed indices, by about 10 per cent. The maximum index can be used roughly to separate narrow and wide components of the source, but it is more accurate to do this by finding the minimum level of the modulation in a strong scattering case.)

The index falls as the source gets very close to the Sun (at 195 MHz). This effect has been seen on other sources which get very close to the Sun, and is discussed in § VII below.

3. The cross-correlation between observations at different frequencies is low. Typical cross-correlation functions are shown in Figure 7.

4. The distribution of fluctuation intensities fits the Rice-squared distribution moderately well. In some cases the distributions are more peaked than the Rice-squared distribution. This is especially notable at 430 MHz (see Fig. 7).

The observations are characteristic of Regions III and IV: the index is on the order of unity and the spectrum width increases with  $\lambda$ . In Figure 11 (see below) the 3C 273 points are reminiscent of the case  $\eta > 1$  (see Fig. 3 of [I]); however, there are only three points, and the error bars just allow one to say that  $f_2$  is proportional to  $\lambda$  over the complete range of observing wavelength. This suggests that 611 MHz is in Region IV and 195 MHz is in Region III, with  $\phi_{611}$  ( $= \phi_0$  at 611 MHz) only a little above unity. The probability distributions of Figure 7 are consistent with this interpretation.

There is no unique way to combine cases (a) and (b), even under the assumption that the scale is independent of  $\epsilon$ . (We have no evidence to the contrary for this.) A reasonable compromise is to say that in case (a)  $\nu_3 \approx 430$  MHz ( $\nu_3 =$  boundary frequency between Regions I and II; see eq. [35] of [I]). The parameter  $\nu_3$  stays constant as we move into case (b); 195 MHz is above the boundary line and is in Region III, while 611 MHz is below and in Region IV. The three spectra in Figure 4 are curved in a way consistent with this hypothesis. The 195 MHz spectrum is slightly concave down, whereas the 430 and 611 MHz spectra are concave up. We may imagine that the progression toward the Gaussian shape (characteristic of Region III) begins to show on the 195 MHz spectrum.

The major inconsistency in relating the observations to the thin-screen theory is the lack of a deep depression near zero frequency in the weak scattering spectra. The expected depression is partly filled in by the geometric effect discussed in [I], § IX: even if the solar wind had a truly uniform radial velocity, the projected transverse velocities across the rays would vary as  $\cos \beta$ , where  $\beta$  is the angle between the ray and the radius vector from the Sun. In § VIII below it is shown that the screen can be regarded as that part of the ray with  $\beta < 30^\circ$ . The geometric effect thus should be rather small and probably does not explain all the observed smoothing. The solar-wind velocity is known to be irregular near Earth and undoubtedly is irregular close to the Sun; this may also explain some of the observed spectral smoothing.

The scattering screen theory is very rich, and our observations have evidently not allowed all facets of it to be explored. The observations should clearly be extended, to both lower and higher frequencies, to smaller elongations, and to a more complete coverage of the interesting intermediate ranges.

#### V. PARAMETERS OF THE SCREEN

##### a) Distance

The strict heliocentric character of the scintillations implies very strongly that the diffracting region is the outer solar corona. Various arguments have also been used to show that the diffracting region cannot be in the ionosphere (Hewish *et al.* 1964), and in [I], § VI, it is demonstrated that the screen is at least 0.3 a.u. away. In the present case it is possible to exclude the ionosphere solely from internal considerations. At 195 MHz we were illuminating about 250 m of the dish; the scale of the ground pattern must be greater than this or the scintillations would be washed out. We have some observations in Region IV where the scale on the ground is about  $\frac{1}{5}$  the scale in the screen and the scintillations are still strongly developed (cf. Fig. 4 at 195 MHz). Thus:  $a > 5 \times 250 \text{ m} = 1.25 \text{ km}$ ; and, at 430 MHz,  $z \approx z_0 = 2\pi a^2/\lambda > 14000 \text{ km}$ .

The magnetopause and the standing shock wave formed by the solar wind are heliocentric as viewed from Earth. Their properties, however, can hardly vary rapidly enough to produce the rapid change in scintillations with elongation.

It is clear that fluctuations in density of the outer corona and the solar wind are responsible for the scintillations. We shall use  $z = 1 \text{ a.u.}$

##### b) Scale

It is possible to make two independent estimates of the scale of the screen, by estimating (1) the Fresnel distance  $z_0$ , and (2) the velocity of the solar wind.

1. As discussed above, we adopt  $\nu_3 \approx 430 \text{ MHz}$ . Setting  $z_0 = 1 \text{ a.u.}$  at 430 MHz gives  $a \approx 130 \text{ km}$ . The scale is proportional only to  $\sqrt{\nu_3}$ , and so is insensitive to errors in its estimation.

2. In Region II the scintillation spectrum on the ground is the same as the phase fluctuation spectrum at the screen. This is only true to order  $\sqrt{z_0/z}$ , however, and cannot be taken too literally for our observations. The second moment of the spectrum, however, is an insensitive parameter and especially is insensitive to the exact shape of the low-wavenumber components. We assume that our typical value, 0.6 c/s, is appropriate for the phase fluctuations.

The solar wind has a typical velocity of 400 km/sec in the vicinity of Earth. Calculations by Whang and Chang (1965) indicate that the velocity is smaller by a factor of about 1.14 at  $r = 0.34 \text{ a.u.}$  ( $\epsilon = 20^\circ$ ). We thus adopt the velocity  $u = 350 \text{ km/sec}$  as being characteristic for our observations. This is the mean velocity of the electrons and is assumed to be radial. We assume that all irregularities in the solar wind have the same motion, so that they move transverse to the line of sight with this velocity. An early suggestion by Hewish *et al.* (1964) was that the irregularities move with constant angular velocity rather than radially; however, our observations do not support this hypothesis and we shall not use it.

We thus estimate  $a$  by taking  $f_2 \approx 0.6 \text{ c/s}$  and  $u = 350 \text{ km/sec}$ :  $a = u/2\pi f_2 \approx 90 \text{ km}$ . We adopt the average value, 110 km, as the scale. This value is very close to that derived by Hewish *et al.* (1966), who found  $a = \xi_0/\sqrt{2} \approx 100 \text{ km}$ , by observations at 3.7 m at two stations separated by 53 km.

Estimates (1) and (2) are very close; each is within the uncertainty of the other. This suggests that the solar wind is not strongly anisotropic and does not consist of long spiral filaments such as would be produced by isolated jets on the photosphere. For, in this case, the proper velocity to introduce would be comparable to the Alfvén speed,

which is much less than the solar-wind velocity. We conclude, in agreement with the recent discussion by Hewish *et al.* (1966), that the irregularities move radially.

Even though the particles and the irregularities move radially, the magnetic field lines will be spirals. If the magnetic field is convected round with the Sun, it will attain those spirals which agree with the radial solar wind (Parker 1958; Wilcox and Ness 1965). Particles from solar flares are moving at speeds well above that of the solar wind; they must move along the magnetic field and cannot come out radially. This, of course, explains the east-west asymmetry of solar-terrestrial phenomena.

The Debye length in the solar wind is about 2 m (assuming  $T \approx 10^5$  ° K and  $n_e \approx 100$  cm $^{-3}$ ), so there is complete charge neutrality on the scale of the irregularities we are observing. The interplanetary magnetic field is typically a few gammas. If we assume it is

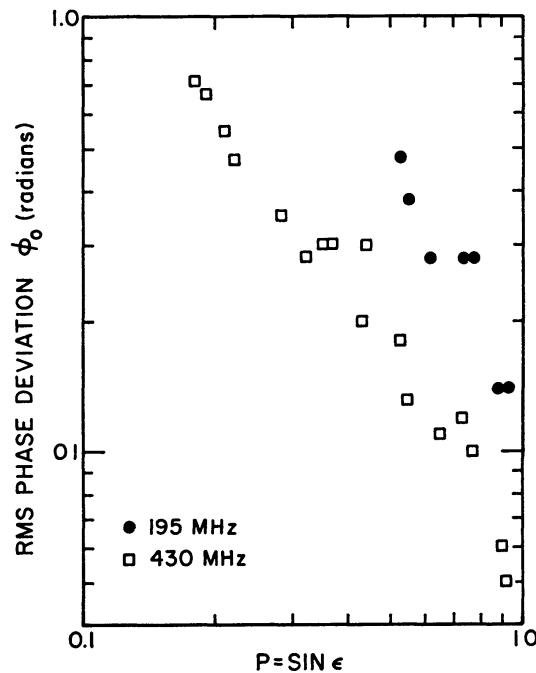


FIG. 8.—The rms phase deviation versus  $p = \sin \epsilon$ ; computed from observations of 3C 273 during September–November, 1965; 430 MHz (squares) and 195 MHz (dots).

$10^{-4}$  gauss at  $R = 80 R_{\odot}$ , then a proton at  $10^5$  ° K has a radius of gyration of about 40 km, or  $\frac{1}{3}$  the scale of the irregularities. This suggests that the irregularities are limited in size by the proton gyroradius.

### c) Phase and Electron Density Fluctuations

The observed curves of  $m$  versus  $p$  in Figure 5 are used to estimate  $\phi_0$ . At both 195 and 430 MHz the maximum values of the index are reduced below unity, mainly because 3C 273B is only a small fraction of the total source (see § IV above). Therefore we first define  $m_{\max}$  as 0.10 and 0.17 for 195 and 430 MHz, respectively, and compute  $\phi_0$  from the ratio  $m/m_{\max}$ . At 195 MHz the scattering is in Region II (for  $\epsilon > 20^\circ$ ), and we use the formula  $m/m_{\max} \approx 2^{1/2} \phi_0$ . At 430 MHz the scattering is near the boundary between Regions I and II, and we assume that the formula  $m/m_{\max} \approx 1.2 \phi_0$  is approximately correct. Use of these two formulae gives the values of  $\phi_0$  shown in Figure 8.

The 430 and 195 MHz points in Figure 8 should be separated by a factor of  $\frac{4.30}{1.95} = 2.2$ , whereas the actual separation is about 2.7. It is not clear where this discrepancy comes from, but in any event it is not important in the present context.

The phase correlation function is given by the electron density correlation function according to equation (48) of [I]. For an isotropic Gaussian electron density correlation function this relation becomes (for  $r_x = 0$ )

$$\phi_0 = (2\pi)^{1/2} r_e \lambda (aL)^{1/2} \Delta n, \quad (2)$$

where  $r_e = 2.82 \times 10^{-13}$  cm,  $L$  is the thickness of the screen, and  $\Delta n \equiv \langle (\Delta n_e)^2 \rangle^{1/2}$ . We adopt the values  $a = 110$  km, and  $L = (2/\sqrt{3}) \sin \epsilon$  a.u., which restricts the screen to a  $60^\circ$  conical sector centered on the Sun. This "screen" is discussed in § VII below.

Values of  $\Delta n$  have been computed from equation (2), using the values of  $\phi_{430}$ , from Figure 8, and they are shown in Figure 9. The formula  $\Delta n = 0.14 r^{-2}$  cm $^{-3}$  (with  $r$  in

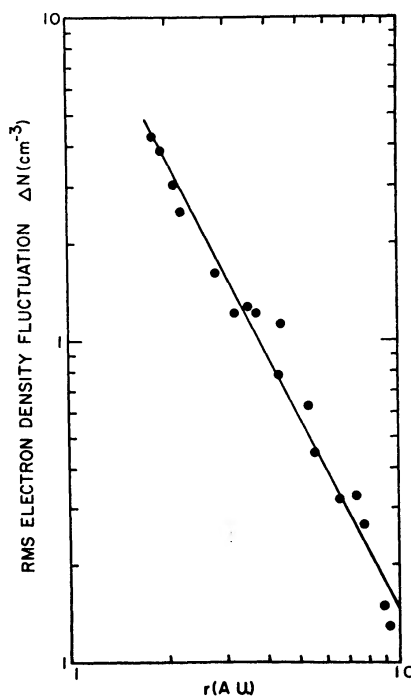


FIG. 9.—The rms fluctuation in electron density versus radial distance from Sun; computed from the 430 MHz points in Fig. 8.

astronomical units) has also been drawn in Figure 9. The measured points have a fairly close fit to this inverse square dependence. The scatter of the points around the line is partly due to experimental uncertainties, but much of it is genuine and corresponds to the large day-to-day fluctuations in the observed index.

Slee (1961) found  $\Delta n \sim r^{-2.3}$ , although his method of reduction was rather different from ours. His measurements were made during sunspot maximum (1958) and apply to the equatorial region. Our measurements were made near sunspot minimum and also apply to the equatorial region.

A rough estimate of the mean electron density  $n_e$  may be taken as  $n_e = 6r^{-2}$  elec/cm $^3$ . This fits the model developed by Ingham (1961) to interpret the zodiacal light at  $r \approx 0.1$ , and gives 6 electrons/cm $^3$  in the vicinity of Earth, which is reasonable in view of recent space-probe measurements. The ratio  $\Delta n/n_e$  is thus about 0.02, and is constant for  $0.2 < r < 0.9$ .

Hewish *et al.* (1966) have reported observations of the source 3C 48 at  $\lambda = 3.7$  m, using two antennas separated by 53 km. They assumed in interpreting the observations

that the source is a point source and that the scattering is in Region II. Our results show that their observations were partly in Region III, however, and their discussion of phase and electron density fluctuations should be repeated.

Figure 8 shows that  $\phi_0 = 1$  at  $\epsilon \approx 30^\circ$ , for  $\lambda = 3.7$  m. Thus the scattering was in Region III from about April 1 to May 15. This agrees with their curve 2(b), which seems to show a flattening from roughly April 1 to May 15. During this period, however, the index ( $F$ ) is on the order of 0.3 instead of 1.0. We suggest that the scintillations are reduced because of the finite screen thickness (see § VII; at  $\lambda = 3.7$  m,  $L > l_0$ ) together with a rather large angular diameter for 3C 48, at  $\lambda = 3.7$  m. Their estimate of  $\Delta n$  is too small by an order of magnitude because they used  $\phi_0 = 0.2$ , instead of about 2, at  $\epsilon = 20^\circ$ .

#### VI. EXTENDED SOURCE AND DIAMETERS OF 3C 138 AND 3C 273

A source which is extended in angle produces overlapping diffraction patterns on the ground (Briggs 1961). The net pattern is the convolution of the point-source pattern with the brightness distribution  $b(\zeta)$  of the extended source, and the fluctuation spectrum  $M_{\text{ext}}(q)$  due to the extended source is

$$M_{\text{ext}}(q) = M(q) |V(qz)|^2, \quad (3)$$

where  $M(q)$  is the spectrum due to the point source and  $V(kx)$  is the usual (complex) visibility function of the source [I, § VI]. Restoration of a brightness distribution from measurements of  $M_{\text{ext}}$  and  $M$  is analogous to a restoration from the diffraction pattern produced by a lunar occultation. In the latter case the point-source response is known a priori and the complex  $V(qz)$  can be found. In the scintillation case the point-source response is random and only the magnitude  $|V(qz)|$  can be found. The information is the same as that obtainable from an intensity interferometer.

Consider a Gaussian source  $b(\zeta) = e^{-(\zeta/\zeta_0)^2/2}$ , with half-power angular width  $\psi = 2.36\zeta_0$ . If this source were convolved with a Gaussian pattern on the ground, there would result the Gaussian spectrum

$$M_{\text{ext}}(q) = e^{-(q/q_2)^2/2} e^{-(q\zeta_0)^2},$$

where  $q_2$  is the intrinsic width (seen with a point source). The width of  $M_{\text{ext}}(q)$  is  $q_2[1 + 0.36(z\psi q_2)^2]^{-1/2}$  and the index is reduced below the point-source value ( $m_0$ ) by  $m/m_0 = [1 + 0.36(z\psi q_2)^2]^{-1/4}$ . When  $(z\psi q_2)^2 \ll 1$  the source is equivalent to a point source. When  $z\psi q_2 \sim 1$  the spectrum becomes narrower and the index is reduced, and when  $(z\psi q_2)^2 \gg 1$  the width approaches the value due to the source alone, but the scintillations disappear: width  $\sim 1.67(z\psi)^{-1}$  and  $m/m_0 \sim 1.29(z\psi q_2)^{-1/2}$ . The spectrum width is a more sensitive and more useful measure of source diameter than is the index; for the latter is a rather slowly varying function, and furthermore cannot be used without first estimating  $q_2$ . (In two dimensions the variation is faster: a circular Gaussian source seen through an isotropic Gaussian screen gives  $m/m_0 \sim 1.29[z\psi q_2]^{-1}$ .)

As an illustration of these ideas, we show in Figure 10, *a-c*, the spectra for two sources, 3C 138 and 3C 273. The 3C 273 curves have already been discussed in § III. The 3C 138 curves come from 5 min of data at 195 and 430 MHz, and from 160 sec of data at 611 MHz. In each case the resolution is about 0.2 c/s. The diagram in Figure 10, *d*, shows the relative positions of the two sources with respect to the Sun and the ecliptic. They are both about  $7^\circ$  from the Sun. The line through 3C 273 indicates the axis connecting the two major components. There was no unusual solar activity on the days prior to the observations. Our experience suggests that orientation around the Sun is not important, and that no significant differences in spectrum could come from the sources being on opposite sides of the ecliptic. We believe that the spectrum differences between the two sources are real and are characteristic of the sources.

At 195 MHz the 3C 138 spectrum shows a definite break at  $f \approx 2$  c/s, and for  $f \geq 1.5$  c/s the curve is well fit by a steep exponential of width  $f_2 = 1.1$  c/s. At 430 and 611 MHz the significant portions of the curves are similar. The second moments of all six curves are shown in Figure 11.

The simplest interpretation of Figures 10 and 11 is that 3C 273 is a point source and generates the point-source spectrum  $M(q)$ . 3C 138, then, has a finite disk which generates the steep spectrum for  $f \geq 1.5$  c/s. Since we have no a priori knowledge of  $M(q)$ , it may well be that it is different (flatter) than the 3C 273 curves. The 3C 138 spectrum, however, shows a break at  $\sim 2$  c/s at 195 MHz, and we interpret this as being due to the finite diameter disk. At the two higher frequencies the break presumably is obscured by the noise.

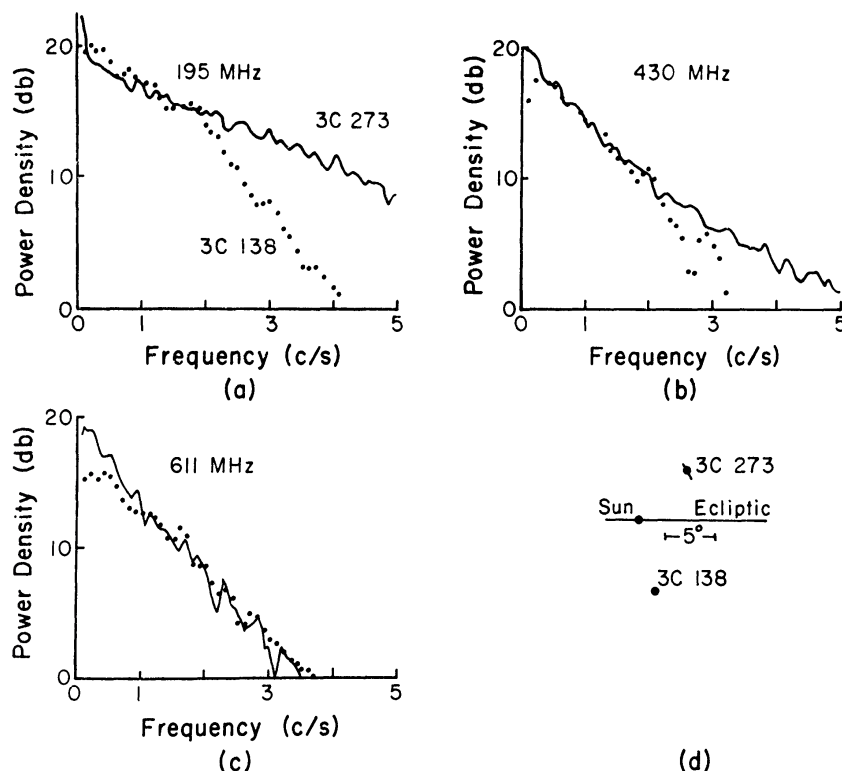


FIG. 10.—Scintillation spectrum of 3C 138, June 13, 1965 (*dotted curves*) and 3C 273, October 3, 1965 (*full-line curves*) at (a) 195 MHz, (b) 430 MHz, (c) 611 MHz. Both sources are about  $7^\circ$  from the Sun. (d) The relative positions of the two sources.

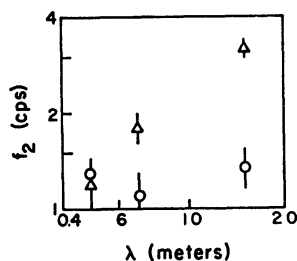


FIG. 11.—(Square root) second moment of scintillation spectrum. *Triangles*: 3C 273, Oct. 3, 1965,  $\epsilon = 7^\circ$ . *Circles*: 3C 138, June 13, 1965,  $\epsilon = 7^\circ$ .

A bell-shaped brightness distribution  $b(\zeta) = [1 + 4(\zeta/\psi)^2]^{-1}$ , with  $\psi$  the half-power width, has an exponential visibility function:  $|V(qz)|^2 = (\pi\psi/2)^2 e^{-qz\psi}$ . As a function of frequency this may be written  $e^{-(f/f_s)^2}$  and the source width is

$$\psi = \frac{u}{\pi z f_s \sqrt{2}}. \quad (4)$$

We estimate the diameter of 3C 138 from equation (4) by using  $u = 350$  km/sec,  $z = 1$  a.u., and  $f_s = 1.1$  c/s. This gives  $\psi \approx 0''.1$ , which is much smaller than the value ( $\sim 0''.5$ ) reported by Anderson, Donaldson, Palmer, and Rowson (1965) from observations made with a two-element interferometer at the somewhat higher frequency 408 MHz.

A position angle may be derived for our observation by assuming a radial motion for the irregularities. This gives P.A. =  $015^\circ$ .

The 3C 273 curves are very smooth and show no signs of a sharp cutoff below 10 c/s. This suggests strongly that the disk is so narrow that the cutoff frequency is above 10 c/s, so we estimate the diameter as  $\psi \leq 0''.02$ , at P.A.  $160^\circ$ . This limit is nearly an order of magnitude smaller than the limit set by Adgie *et al.* (1965) for the components of 3C 273B, at  $\lambda = 21$  cm.

Adgie *et al.* (1965) interpret their interferometer observations in terms of two "point" sources for 3C 273B; each of them is less than  $0''.1$  in diameter, and their separation is  $0''.4$  if they are separated along the line joining *A* to *B*, at P.A.  $044^\circ$ . Now the visibility function for a double source of equal components is a cosine function. A separation of  $0''.4$  along the solar wind thus would have produced a null in the scintillation spectrum at about 0.6 c/s, with further nulls at 1.8, 3.0, . . . c/s. We see no signs of this modulation on our spectra, or of regular modulation of any other period. In view of our discussion above, however, concerning the missing depression in the point-source spectrum in weak scattering, it would not be surprising if cosine shapes were smoothed out. We cannot make detailed brightness distribution calculations until this smoothing is understood in more detail.

An elementary derivation of equation (4) was given in an earlier paper (Cohen, Gundermann, Hardebeck, Harris, Salpeter, and Sharp 1966).

#### VII. EFFECTS OF FINITE SCREEN THICKNESS

The screen that we have been discussing is, of course, the solar wind, and whether or not it can be regarded as "thin" depends on the particular parameter being investigated and upon the scattering regime [I, § VII] (but see note added in proof in Paper I on p. 444). Each line element along a ray contributes to  $\phi_0^2$  according to  $(\Delta n)^2$ . If  $\Delta n$  varies as  $r^{-2}$ , it can be shown that about  $\frac{2}{3}$  the total contribution to  $\phi_0^2$  comes from the section with  $\beta \leq 30^\circ$  ( $\beta$  is the angle between the ray and the radius vector from the Sun). We therefore adopt this region as the "screen," and have  $L = (2/\sqrt{3}) \sin \epsilon$  a.u. For the values of  $\epsilon$  considered in this paper, we have  $\lambda \ll a \ll L \ll z$ , but we do not always have  $L \ll l_0$ , or even  $L \ll z_0$ . The screen is not thin for all purposes.

At 195 MHz,  $z_0 = ka^2 = 0.39$  a.u., and  $L > z_0$  for  $\epsilon > 20^\circ$ . But  $\phi_{195} = 1$  rad at  $\epsilon \approx 15^\circ$ , so for  $\epsilon < 15^\circ$ ,  $L$  must be compared with  $l_0$ , not  $z_0$ . From Figure 8,  $\phi_{195} \approx (\epsilon/15^\circ)^{-2}$  so that  $L > l_0$  also. At 430 MHz,  $L < z_0$  for the observations reported here, and  $L < l_0$  for  $\epsilon$  bigger than  $4^\circ$  or  $5^\circ$ .

Having  $L > z_0$  for  $\epsilon > 15^\circ$  means that there is an amplitude as well as a phase variation at the bottom of the screen. This amplitude fluctuation in any event is small, since  $\phi_0 < 1$ . The net effect on the scintillations on the ground should be small.

Having  $L > l_0$  for  $\epsilon < 15^\circ$  means that the amplitude fluctuations will be large well inside the screen. The radiation inside the screen is also spread through the angle  $\langle \theta^2 \rangle^{1/2}$  which is about  $1''$  for a rms phase deviation of 2 rad [I, eq. (6)]. The exact shape the

spectrum might take seems difficult to estimate since it is not clear what form any cutoff would take, and the increasing  $\phi_0$  requires the spectrum to get wider. We conjecture, however, that the net effect would be to reduce the index below its normal, i.e., thin-screen, value.

We believe that this effect is responsible for the rapid drop in index which occurs when the source comes close enough to the Sun. The observed drop in index is similar for all sources which we have observed within about  $8^\circ$  from the Sun. It has been reported by Hewish and Okoye (1965) for the Crab Nebula at 38 MHz. It can be seen in Figure 5, where (at 195 MHz) the index falls for  $\epsilon \lesssim 8^\circ$ , where  $\phi_{195} \approx 2.5$  rad. At 430 MHz the index has not fallen by  $\epsilon \approx 6^\circ$ , where  $\phi_{430} \approx 2$  rad. The lack of a drop here, however, is marginal. The drop has been seen on other sources, closer to the Sun, at all 3 observing frequencies.

Hewish and Okoye (1965) ascribe the effect to the finite size of the source, combined with the decreased scale on the ground, when  $\phi_0 > 1$ . They use the thin-screen theory, which gives the scale as  $\approx a/\phi_0$ . If this explanation were correct we would expect different sources to show the drop in index at different positions, according to their diameters. However, we observe the drop to occur at roughly the same elongation for all these sources, although the determination is rather inaccurate. Also the drop in index should be due to the high wavenumber components being cut out of the spectrum, but our measured spectra show no signs of this. Figure 4, *a*, was taken at  $\epsilon = 7^\circ$ , when the index had already begun to fall, but the spectrum shows no high-frequency cutoff. The reduction in index appears to be due to a general lowering (or perhaps a tapered lowering) of the whole spectrum.

Another effect of the finite screen thickness is the dispersion in transverse velocities due to the radial motion of the irregularities as already discussed in § IV above. This dispersion should tend to smooth out the observed fluctuation spectrum by shifting some energy toward lower frequencies. This effect will be seen in frequency ( $f$ ), but not in wavenumber ( $q$ ), spectra. Thus, observations at several ground stations should be able to see the dispersion directly.

In order to get unambiguous determinations of brightness distribution to high resolution, the observations should be made with  $\phi_0 \gg 1$  and  $z \gg l_0 \gg L$ . A high frequency is needed for this. For example, if 611 MHz is used with  $\phi_0 = 10$  rad, all the conditions will be satisfied, but the observations will have to be made at  $\epsilon \approx 2^\circ$ , which is difficult. These numbers will have to be changed if the scale,  $a$ , is found to change substantially as the Sun is approached.

We are grateful to D. E. Harris for much assistance with the observations, to M. Hurley for assistance with the calculations and data reductions, and to E. E. Salpeter for many helpful discussions and suggestions. The Arecibo Ionospheric Observatory is operated by Cornell University with the support of the Advanced Research Projects Agency under a research contract with the Air Force Office of Scientific Research.

## APPENDIX

The probability distribution of the length of a vector that is the sum of a constant vector and a Rayleigh-distributed vector is called a Rice distribution (Rice 1954). A Rayleigh-distributed vector is identical to a vector that is the sum of two perpendicular vectors the lengths of which have identical and independent Gaussian distributions with means zero. If  $Z$  is Rice-distributed, then

$$F_Z(z) \equiv \text{probability } \{Z < z\} \equiv \int_{-\infty}^z f_Z(y) dy$$

where

$$f_Z(y) = (y/\sigma^2) \exp [-(y^2 + c^2)/2\sigma^2] I_0 [cy/\sigma^2]; \quad y \geq 0 \\ = 0 \text{ otherwise}$$

and

$\sigma^2$  = variance of Gaussian components

$c$  = length of constant vector

$I_0(x) \equiv J_0(ix)$  is a modified Bessel function of the first kind of order zero.

If one is interested in the distribution of  $Z^2$  (intensity) rather than that of  $Z$ , then the transformation  $X = Z^2$  may be made, that is,

$$\int_{-\infty}^x f_X(y) dy \equiv F_X(x) \equiv \text{prob.} \{X < x\} = \text{prob.} \{Z^2 < x\} = \text{prob.} \{Z < \sqrt{x}\} \\ = \int_{-\infty}^{\sqrt{x}} f_Z(y) dy = \int_0^{\sqrt{x}} f_Z(y) dy = \int_0^x f_Z(\sqrt{y}) \frac{1}{2\sqrt{y}} dy,$$

so that

$$f_X(y) = f_Z(\sqrt{y}) \frac{1}{2\sqrt{y}} = \left( \frac{1}{2\sigma^2} \right) \exp [-(y + c^2)/2\sigma^2] I_0(c\sqrt{y}/\sigma^2) \quad y \geq 0 \\ = 0 \text{ otherwise.}$$

The moments may be calculated directly from the definition of  $X$ , that is,

$$X = (c + A)^2 + B^2,$$

where  $A$  and  $B$  have independent and identical Gaussian distributions with means zero and variances  $\sigma^2$ . The first three central moments are

$$\langle X \rangle = c^2 + 2\sigma^2,$$

$$\sigma_X^2 = \langle (X - \langle X \rangle)^2 \rangle = \langle X^2 \rangle - \langle X \rangle^2 = 4\sigma^2(c^2 + \sigma^2),$$

and

$$\langle (X - \langle X \rangle)^3 \rangle = 8\sigma^4(2\sigma^2 + 3c^2).$$

The probability density  $f_X(y)$  may be reduced to a standard form by the transformation  $Y = (X - \langle X \rangle)/\sigma_X$ , so that a one-parameter family of curves with  $S = c/\sigma$  as the parameter results. It is occasionally more convenient to use the skewness parameter [I, § IV]

$$\xi_3 = \frac{\langle (X - \langle X \rangle)^3 \rangle^2}{4 \langle (X - \langle X \rangle)^2 \rangle^3} = \frac{(2 + 3S^2)^2}{4(1 + S^2)^3}$$

to specify a particular member of the family. The probability density of the standard variable becomes

$$f_Y(y) = (S^2 + 1)^{1/2} \exp \{ - [ (S^2 + 1)^{1/2} y + 1 + S^2 ] \} \\ I_0 \{ S [ 2 (S^2 + 1)^{1/2} y + S^2 + 2 ]^{1/2} \}; \quad y \geq -\frac{2 + S^2}{2(1 + S^2)^{1/2}} \\ = 0 \text{ otherwise.}$$

As the length of the constant vector approaches zero,  $S \rightarrow 0$ ,

$$f_Y(y) \rightarrow e^{-[y+1]} ; \quad y \geq -1 \\ \rightarrow 0 \text{ otherwise ,}$$

and  $\xi_3 \rightarrow 1$ .

If the constant vector is very large compared to the variance of the Gaussian components,  $S \rightarrow \infty$ , and

$$f_Y(y) \rightarrow S \exp(-Sy - S^2) I_0[S(2Sy + S^2)^{1/2}] .$$

The asymptotic expansion for  $I_0(x)$  (Dwight 1957),

$$I_0(x) \sim \frac{1}{\sqrt{(2\pi x)}} e^x ,$$

may be used, so that

$$f_Y(y) \rightarrow \frac{1}{(2\pi)^{1/2} [2(y/S) + 1]^{1/4}} \exp \left\{ S^2 \left[ -1 - \frac{y}{S} + \left( 2 \frac{y}{S} + 1 \right)^{1/2} \right] \right\} \\ \rightarrow \frac{1}{(2\pi)^{1/2}} e^{-y^2/2} ,$$

which is the standard form for a Gaussian distribution. The skewness factor also approaches zero, as it should, since a Gaussian is symmetric.

#### REFERENCES

- Adgie, R. L., Gent, H., Slee, O. B., Frost, A. D., Palmer, H. P., and Rowson, B. 1965, *Nature*, **208**, 276.  
 Anderson, B., Donaldson, W., Palmer, H. P., and Rowson, B. 1965, *Nature*, **205**, 375.  
 Blackman, R. B., and Tukey, J. W. 1958, *The Measurement of Power Spectra* (New York: Dover Publications).  
 Briggs, B. H. 1961, *Geophys. J.*, **5**, 306.  
 Cohen, M. H. 1965, *Nature*, **208**, 277.  
 Cohen, M. H., Gundermann, E. J., Hardebeck, H. E., Harris, D. E., Salpeter, E. E., and Sharp, L. E. 1966, *Science* **153**, 745.  
 Douglas, J. N. 1964, *I.E.E.E. Trans. Mil Elec*, MIL-8, p. 173.  
 Dwight, H. B. 1957, *Tables of Integrals and Other Mathematical Data* (3d ed.; New York: Macmillan Co.), p. 182.  
 Hewish, A., Dennison, P. A., and Pilkington, D. H. 1966, *Nature*, **209**, 1188.  
 Hewish, A., and Okoye, S. E. 1965, *Nature*, **207**, 59.  
 Hewish, A., Scott, P. F., and Wills, D. 1964, *Nature*, **203**, 1214.  
 Ingham, M. F. 1961, *M.N.*, **122**, 157.  
 Parker, E. N. 1958, *Ap. J.*, **128**, 664.  
 Rice, N. 1954, *Selected Papers on Noise and Stochastic Processes* (New York: Dover Publications), p. 238.  
 Salpeter, E. E. 1967, *Ap. J.*, **147**, 433 ([I]).  
 Slee, O. B. 1961, *M.N.*, **123**, 223.  
 Whang, Y. C., and Change, C. C. 1965, *J. Geophys. Res.*, **70**, 4175.  
 Wilcox, J. M., and Ness, N. F. 1965, *J. Geophys. Res.*, **70**, 5793.